Carboxymethyl Tamarind-g-poly(acrylamide)/Silica: A High Performance Hybrid Nanocomposite for Adsorption of Methylene Blue Dye

ARTICLE *in* INDUSTRIAL & ENGINEERING CHEMISTRY RESEARCH · NOVEMBER 2012

Impact Factor: 2.59 · DOI: 10.1021/ie301134a

I&EC research
Industrial & Engineering Chemistry Research

Article

pubs.acs.org/IECR

Carboxymethyl Tamarind-g-poly(acrylamide)/Silica: A High Performance Hybrid Nanocomposite for Adsorption of Methylene Blue Dye

Sagar Pal,*[,†] S. Ghorai,[†] C. Das,[†] S. Samrat,[†] A. Ghosh,[‡] and Asit Baran Panda*[,§]

[†]Polymer Chemistry Laboratory, Department of Applied Chemistry, Indian School of Mines, Dhanbad-826004, India

[‡]Department of Pharmaceutical Sciences, Birla Institute of Technology, Mesra, Ranchi-835215, India

[§]Disciplines of Inorganic Materials and Catalysis, Central Salt and Marine Chemicals Research Institute (CSIR-CSMCRI), Bhavnagar-364021, India

Supporting Information

ABSTRACT: Here, synthesis of an efficient nanocomposite based on a polyacrylamide grafted carboxymethyl tamarind (CMT-g-PAM) and a SiO_2 nanoparticle is presented. The synthesized nanocomposites are characterized using FT-IR, SEM, TEM, ^{13}C NMR, elemental analysis, viscosity, rheological measurement, and molecular weight determination. Various characterizations reveal the existence of an excellent polymer matrix−nanoparticle interaction, which is at a maximum when 1.5 wt % of SiO_2 is introduced in the polymer matrix (i.e., CMT-g-PAM/SiO_2-3). Nanocomposites show tremendous methylene blue (MB) dye adsorption capacity, because of their higher hydrodynamic radius as well as hydrodynamic volume, which originates from proper polymer matrix−SiO_2 nanoparticle interaction. CMT-g-PAM/SiO_2-3 exhibited a maximum adsorption capacity (Q_{max}) of 43.859 $mg \cdot g^{-1}$. The adsorption behavior of the nanocomposite shows that adsorption kinetics and isotherms are in good agreement with pseudo-second-order and Langmuir equations, respectively. Negative values of ΔG° confirmed the spontaneous nature of adsorption. Further, desorption experiments affirmed that the developed nanocomposite has excellent regenerative efficacy.

INTRODUCTION

Hybrid inorganic−organic nanocomposites, composed of inorganic nanoparticles and functional polymers, are a novel and unique class of materials. In recent years, they have become more important because of their improved properties, which are derived from synergistically combined properties of inorganic particles and organic polymers.[1−5] The properties of nanocomposite materials depend not only on the individual components but also on their morphological and interfacial characteristics. Titanium nanoparticles have been extensively utilized as the inorganic component in nanocomposites.[2,6] However, recently more attention has been focused on synthetic silica nanoparticles, because of their potential as surface-modified substrates in various applications.[7−9] Monodispersed silica particles with uniform size and shape have wide industrial applications in industries manufacturing pigments, pharmaceuticals, ceramics, and catalysts.[10]

Water is the most essential prerequisite for our civilization to flourish. Availability of pure water is one of the most important requirements for a sound public health system. Dye industry effluents are the largest contributor to textile effluent and color wastewater.[11] The discharge of color wastewater from textile industries has a serious destructive impact on the environment and can introduce the potential danger of bioaccumulation.[12,13] Various techniques such as reverse osmosis,[14] activated carbon adsorption,[15] and photocatalytic degradation of dyes,[16,17] have been proposed for the treatment of textile industry wastewater. Efficient adsorption of dye molecules onto adsorbent is also an effective way for the removal of dyes from wastewater.[11,13] The main advantage of adsorption is its low generation of residues as well as the possibility of recycling and of adsorbent.[18] The use of cheap and biodegradable adsorbents could be an efficient tool to minimize the environmental impact.[19−26] In recent years, particular attention has been focused on biosorbents for removal of dyes.[19,27−31] Modified polysaccharides, in particular polyacrylamide grafted polysaccharides and poly(acrylic acid) grafted polysaccharides are extensively used as flocculants for wastewater treatment as well as drag reducing agents.[32−36] They are efficient flocculants at low doses, controlled biodegradable, shear resistant, inexpensive, and ecofriendly. The polysaccharide based graft copolymers are also used as adsorbents.[28−30] However, they have some limitations such as low surface area, small hydrodynamic radius, and complicated diffusion processes. These drawbacks restrict their use as efficient adsorbent. Introduction of nanoscale filler in the graft copolymer-based matrix may increase the surface area and hydrodynamic radius and therefore can be suitable for use as excellent adsorbent.

The main focus of this manuscript is the development of a high performance nanocomposite based on silica nanoparticles-incorporated polyacrylamide grafted carboxymethyl tamarind (CMT-g-PAM) as well as its application in flocculation and adsorption. Tamarind kernel polysaccharide (TKP) is a cheap polysaccharide having interesting properties. It is used as biomaterial,[37] as well as a food additive in food industry.[38]

Received: May 2, 2012
Revised: November 8, 2012
Accepted: November 10, 2012
Published: November 10, 2012

dx.doi.org/10.1021/ie301134a | *Ind. Eng. Chem. Res.* 2012, 51, 15546−15556

Table 1. Synthesis Details, Viscosity, Molecular Weight, and Hydrodynamic Radius of Graft Copolymer and Various Nanocomposites

polymer	amount of nanofiller (wt %)	% grafting/ conversion[a]	intrinsic viscosity (dL/g)	wt av mol wt (g/mol)	hydrodynamic radius (nm)	% adsorption of MB dye
CMT			8.1	1.01×10^6	5.6	58.69
CMT-g-PAM	0	23.7	14.3	5.02×10^6	10.7	72.91
CMT-g-PAM/SiO_2-1	0.5	35.0	24.2	5.84×10^6	15.2	89.42
CMT-g-PAM/SiO_2-2	1.0	46.0	30.1	6.23×10^6	18.5	93.37
CMT-g-PAM/SiO_2-3	***1.5***	***54.7***	***35.2***	***6.88×10^6***	***26.2***	***99.76***
CMT-g-PAM/SiO_2-4	2.0	36.4	32.4	6.10×10^6	23.9	96.48
nano-SiO_2					8.9	84.22

[a]% conversion = (wt of modified polysaccharide − wt of polysaccharide)/(wt of monomer + wt of nanofiller).

Carboxymethyl tamarind[39] is a semisynthetic natural polymer that has a better solubility in aqueous medium as compared to native tamarind gum. This investigation reports on the preparation and evaluation of a natural polymer-based nanocomposite (CMT-g-PAM/SiO_2) as a high performance flocculant as well as an adsorbent for removal of MB dye in aqueous solution that has extensive future utility.

EXPERIMENTAL SECTION

Materials. Carboxymethyl tamarind gum was synthesized in the authors' laboratory.[39] Acrylamide and potassium persulfate were procured from E. Merck, India. Analytical grade acetone and hydroquinone were supplied by S. D. Fine Chemicals, Mumbai, India. All the chemicals were used as received, without further purification. Silica nanoparticles (particle size in the range of 5−12 nm) were purchased from Sigma-Aldrich Chemie GmbH, Steinheim, Germany. Kaolin was supplied by B. D. Pharmaceutical Works Pvt. Ltd., Howrah, India. Methylene blue was procured from Loba Chemie Pvt. Ltd., Mumbai, India.

Synthesis. The polyacrylamide grafted carboxymethyl tamarind gum (CMT-g-PAM) was synthesized (having % *G* = 237% and % GE = 23.7%) by a radical polymerization technique in inert atmosphere of nitrogen using potassium persulfate as initiator.[40] The nanocomposite (CMT-g-PAM/SiO_2) was developed by in situ incorporation of silica nanoparticles onto the polymer matrix. The detailed synthesis procedure is given as follows.

A 1 g portion of CMT was slowly dissolved into 80 mL of distilled water in a three-necked round-bottom flask. The flask was fitted with an electrically operated magnetic stirrer (Tarsons, model: Spinot Digital) and kept in an oil bath, maintained at a temperature of 60 °C, with constant stirring (400 rpm). Afterward, 0.14 mol of acrylamide dissolved in 15 mL of double distilled water was added to the polysaccharide solution and heated to a temperature of 60 °C, with the same stirring speed. At this stage, 0−2 g of nanosilica (Table 1) was added along with 3.7 mM potassium persulfate solution (total volume 5 mL) under constant stirring. The reaction was continued for another 2 h. During the whole reaction, nitrogen gas was purged through the reaction system. The reaction was terminated using a saturated solution of hydroquinone. Thereafter, the reaction mixture was cooled slowly to room temperature and dispersed in acetone. The product was washed with 250 mL of acetone, filtered with Whatmann 41 filter paper, and then dried in an oven at 40 °C for 6 h. Finally, the prepared nanocomposite was pulverized by mortar/pestle, and sieved through a 125 μm sieve. The synthesis parameters are summarized in Table 1.

Characterization. Intrinsic viscosities of CMT, graft copolymer, and nanocomposites were measured at 25 °C using a Ubbelohde viscometer (with capillary diameter of 0.58 mm) in 1 M sodium nitrate solution. Weight average molecular weight was measured using SLS analysis (Zetasizer Nano ZS, Malvern, UK) and hydrodynamic radius was measured using DLS analysis (Zetasizer Nano ZS, Malvern, UK); double distilled water was used as solvent. C, H, N analysis was performed using an elemental analyzer (Perkin-Elmer, Series-II, CHNS/O analyzer-2400). FTIR spectra were measured by FTIR sectrophotometer (model IR-Perkin-Elmer, Spectrum 2000; between 500 and 4000 cm^{-1}). ^{13}C and ^{29}Si MAS nuclear magnetic resonance (NMR) spectra were recorded at 500 MHz on a Bruker Advance II-500 NMR spectrophotometer. Morphological characterization and EDAX analysis were carried out using scanning electron microscopy (SEM, model: JSM-6390LV; JEOL, Japan) and transmission electron microscopy (TEM, model: JEM 2100, JEOL, Japan).

Investigation of Rheological Characteristics. The rheological properties were investigated in the laboratory using a Paar Physica Advanced Rheometer. The temperature of the system was maintained at 25 °C throughout the experiment. The aqueous solutions of CMT (1 wt %), CMT-g-PAM (1 wt %), and the nanocomposites (1 wt %) were prepared by adding the required quantity of polymers/composites slowly to distilled water with continuous stirring (400 rpm for 3 h) using a magnetic stirrer at a temperature of 60 °C.

Biodegradability Study of the Nanocomposite. *By Viscometric Method.* CMT, CMT-g-PAM, and CMT-g-PAM/SiO_2-3 were subjected to biodegradation studies using the viscometric method.[41] The progress of biodegradation was monitored by measuring intrinsic viscosity after a certain interval of time (after every 7 days).

By Colony Growth. A sample film of CMT-g-PAM/SiO_2-3 was inoculated with *Aspergillus niger* on a medium and incubated at surrounding temperature (25−37 ∘C) for 21 days. The sample was cut (2.5 cm × 2.5 cm) and placed on the surface of mineral salts agar in a Petri-dish having no additional carbon source. Before placing the sample, the Agar surface was cultivated with *A. Niger* from tapioca slices. Afterward, the film was examined for evidence of colony growth.

Investigation of Flocculation Characteristics. The flocculation characteristics of various nanocomposites and parental polymers were investigated using the standard jar test and settling test method. The details of the experimental procedure have been given in the Supporting Information.

Adsorption Experiments. The adsorption experiment of an aqueous solution of MB dye was performed on a

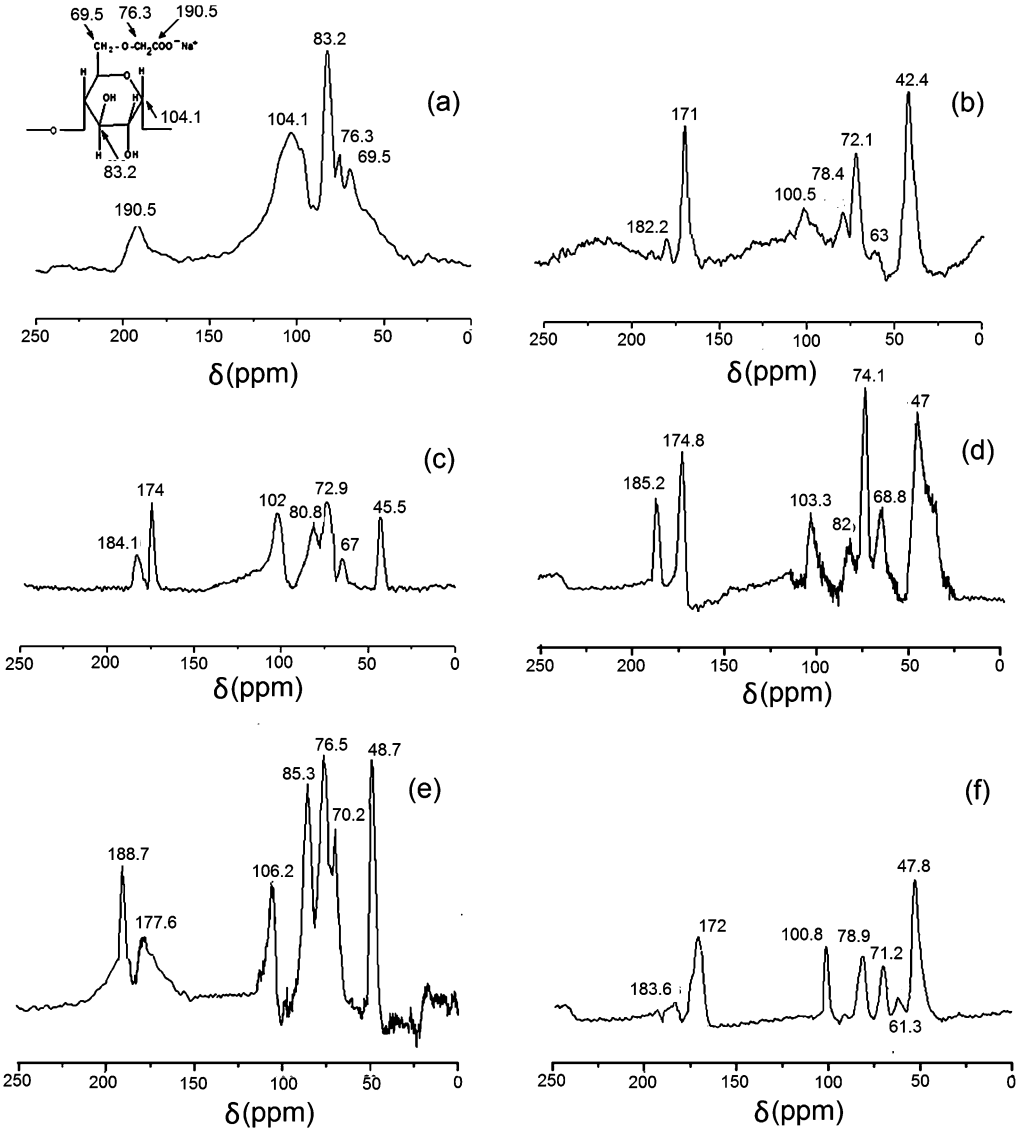

Figure 1. ^{13}C NMR spectra of (a) CMT, (b) CMT-g-PAM, (c) CMT-g-PAM/SiO_2-1, (d) CMT-g-PAM/SiO_2-2, (e) CMT-g-PAM/SiO_2-3, and (f) CMT-g-PAM/SiO_2-4.

thermostatted orbital shaker (Rivotek, Kolkata, India). The details of the experimental procedure have been given in the Supporting Information. The percentage adsorption of dye was calculated using the following formula:

$$\%\text{adsorption} = \frac{C_0 - C_e}{C_0} 100 \quad (1)$$

and the equilibrium uptake was calculated using the following formula:

$$q_e = (C_0 - C_e) \times \frac{V}{W} \quad (2)$$

where q_e is the equilibrium capacity of MB dye on the adsorbent (mg g^{-1}), C_0 is the initial concentration of MB solution (mg L^{-1}), C_e is the equilibrium concentration of MB solution (mg L^{-1}), V is the volume of MB solution used (L) and W is the weight of adsorbent (g) used. All the batch experiments were carried out in triplicate, and the values reported here are an average of three readings.

Desorption Experiments. To determine the reusability of the nanocomposite as adsorbent, four consecutive adsorption–desorption cycles were performed with pH = 2.5, pH = 7, and pH = 8.5 as stripping solutions. The details of the experimental procedure for the desorption study is discussed in the Supporting Information.

RESULTS AND DISCUSSION

Synthesis. CMT-g-PAM was synthesized using potassium persulfate as the free radical initiator, in nitrogen atmosphere. Table 1 shows the various grades of nanocomposites synthesized by varying nanofiller concentration. The optimization was performed through their percentage of conversion, intrinsic viscosity, rheological characteristics, molecular weight, and hydrodynamic radius. The mechanism by which the graft copolymer-based nanocomposite was developed is based on the fact that potassium persulfate generates free radical sites on the CMT backbone. These free radicals react with monomer (acrylamide) to generate the graft copolymer. It is also presumed that the silica particles are attached with the graft

dx.doi.org/10.1021/ie301134a | Ind. Eng. Chem. Res. 2012, 51, 15546–15556

copolymer matrix through H-bonding between the hydroxyl and amide groups of grafted polymer and the silanol groups of silica particles as proposed in Scheme S1 (Supporting Information).

Explanation of Intrinsic Viscosity, Molecular Weight, and Hydrodynamic Radius. The intrinsic viscosity was measured in 1 M $NaNO_3$ solution and the results are presented in Table 1. The intrinsic viscosity of CMT-g-PAM is higher than that of CMT. This is because of the presence of grafted polyacrylamide chains onto the CMT backbone. Further, the rise in viscosity after incorporation of nanosilica implies better polymer matrix−nanoparticle interaction. It is also observed that with the increase in nanoparticle concentration, viscosity is increased up to 1.5 wt % of SiO_2 concentration in the polymer matrix. However, with further rise in filler concentration, viscosity is decreased. This confirms the optimum interaction at 1.5 wt % of SiO_2 concentration. The weight average molecular weight (M_w) and hydrodynamic radius (R_H) of CMT, CMT-g-PAM, and nanocomposites were determined using SLS and DLS analysis, respectively. It is obvious (Table 1) that the M_w and R_H of CMT-g-PAM are higher compared to that of CMT, because of the presence of grafted polyacrylamide chains. Further, all the grades of nanocomposites have higher M_w and R_H than that of the graft copolymer. This is because of the incorporation of nanofiller onto the surface of graft copolymer matrix.

Elemental Analysis. The elemental analysis (%) of CMT (C, 47.92; H, 6.442; N, 2.057; O, 43.58; S, 0.0), CMT-g-PAM (C, 44.08; H, 7.882; N, 15.18; O, 32.85; S, 0.0) and CMT-g-PAM/SiO_2-3 (C, 43.25; H, 7.45; N, 14.31; O, 34.97; S, 0.0) shows that there is a considerable amount of nitrogen content in the graft copolymer and nanocomposite compared to the CMT. This confirms successful grafting of PAM chains onto CMT. Further, a closure scrutiny reveals that the percentage of O is higher (2.12%) in the nanocomposite, which is mainly because of the presence of silanol−OH groups as well as may be because of the trace amount of moisture.

FTIR Spectroscopy. In the FTIR spectrum of CMT (Figure S1a, Supporting Information), the broad peak at 3298 cm^{-1} and a small peak at 2926 cm^{-1} are attributed to the stretching vibrations of O−H and C−H, respectively. The two bands, close to each other at 1700 cm^{-1}, are attributed to the −COOH and $-COO^-$ groups. The bands at 1050 and 980 cm^{-1} are assigned to CH_2-O-CH_2 stretching vibrations. In the case of acrylamide (Figure S1b, Supporting Information), a broad peak at 3352 cm^{-1} is responsible for the stretching vibration of the N−H bond, a peak at 2813 cm^{-1} is due to C−H stretching vibrations. The band at 1921 cm^{-1} is assigned to C═C stretching vibration. Also the stretching vibration at 1674 cm^{-1} and bending vibration at 1611 cm^{-1} are attributed to amide-1($\nu_{C=O}$) and amide-2 (ν_{NH}), respectively. Finally, a sharp peak is observed at 1429 cm^{-1}, which is due to the C−N stretching vibration. In the FTIR spectrum of CMT-g-PAM (Figure S1c, Supporting Information), it has been observed that there are few additional bands present in comparison with that of CMT. These peaks are assigned to amide-I, amide-II, and C−N stretching vibrations, which confirms grafting of polyacrylamide chains onto the CMT backbone. However, the spectrum of CMT-g-PAM/SiO_2-3 (Figure S1d, Supporting Information) also has few additional peaks compared to graft copolymer. A broad peak at 3724 cm^{-1} is assigned to the silanol−OH group. Peaks at 1110 and 945 cm^{-1} are attributed to Si−O−Si and Si−OH linkages, respectively. The presence of these extra peaks confirms the formation of nanocomposite.

Solid State ^{13}C and ^{29}Si MAS NMR Spectroscopy. The ^{13}C NMR spectrum of CMT (Figure 1a) reveals five distinct peaks. The peak at δ = 190.5 ppm relates to carboxyl carbon of COO^-Na^+ of CMT, while the peak at δ = 76.3 ppm is for the carbon of the chemically inserted $-O-CH_2$ portion of CMT. The peak at δ = 104.1 ppm is for anomeric carbon atom and the peak at δ = 83.2 ppm is for carbon atoms connected by −OH groups (i.e., the carbon atoms in the six-membered ring except anomeric carbon atom). Another peak at δ = 69.5 ppm is attributed to the carbon atom of the CH_2OH group. The ^{13}C NMR spectrum of acrylamide has three major peaks.[32] The peak at δ = 177.3 ppm is from the amide carbonyl carbon. Peaks at δ = 130.5 and 138.2 ppm are for two sp^2 hybridized carbon atoms (i.e., CH_2═CH−). In comparison with CMT, CMT-g-PAM (Figure 1b) has a couple of additional peaks. The peak at 171 ppm is for the amide carbonyl carbon. The peak at δ = 42.4 ppm is for the $-CH_2-CH_2-$ groups which are formed during the polymerization reaction. As seen in the ^{13}C NMR spectra of the acrylamide and graft copolymer, the peaks at δ = 130.5 and 138.2 ppm of two sp^2 hybridized carbon atoms of acrylamide are absent in the graft copolymer. Moreover, one additional peak is observed at δ = 42.4 ppm, which is for sp^3 hybridized carbon atoms (i.e., $-(CH_2-CH)_n$ units in the graft copolymer). Neither CMT nor the acrylamide spectra have this peak. Therefore, the absence of peaks at δ = 130.5 and 138.2 ppm and the presence of a peak at δ = 42.4 ppm are strong evidence of the grafting of polyacrylamide chains onto the CMT backbone. The ^{13}C NMR spectra of all nanocomposites (Figure 1c−f) show the regular shifting of peaks toward higher values. However, CMT-g-PAM/SiO_2-3 has accorded a slightly greater shift in comparison with the other nanocomposites for better distribution of silica in the graft polymer matrix and better interaction with CMT-g-PAM through H-bonding, as evidenced from viscosity, rheological properties, and hydrodynamic radius results.

The solid state ^{29}Si MAS NMR spectrum of the nanocomposite (CMT-g-PAM/SiO_2-3) (Figure S2, Supporting Information) shows three different signals at −95.4, −101.2, and −112.7 ppm which can be assigned to $(-O-)_2Si(OH)_2(Q^2)$, $(-O-)_3Si(OH)(Q^3)$, and $(-O-)_4Si(Q^4)$, respectively. The spectrum is almost identical to the initial silica material, confirming the successful insertion of silica particles onto the surface of the CMT-g-PAM matrix. However, the spectrum of the nanocomposite is noisy, indicating the presence of a large amount of nonsilica mass, that is, polymer.

Scanning Electron Microscopic (SEM) and EDAX Analysis. Figure S3a (Supporting Information) shows the granular morphology of carboxymethyl tamarind, which was drastically converted into a fibrillar morphology after grafting with the polyacrylamide chains (Figure S3b, Supporting Information). However, better matrix coherency is achieved after nanofiller insertion (Figure S3c, Supporting Information). The silica incorporation onto the nanocomposite is further confirmed from the presence of a silicon peak in the EDAX spectra (Figure S4, Supporting Information).

Transmission Electron Microscopic (TEM) Analysis. Figure 2 represents the TEM image of the CMT-g-PAM/SiO_2-3 nanocomposite. From the TEM image, it is evident that the silica particles are quite monodispersed and uniformly distributed throughout the polymer matrix (as marked by white arrows). The figure provides excellent evidence of the

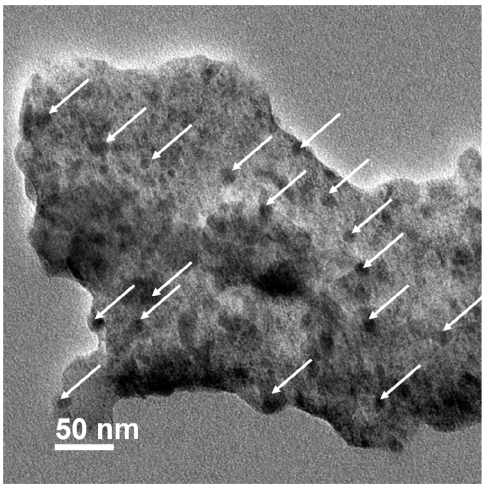

Figure 2. TEM micrograph of CMT-g-PAM/SiO_2-3 nanocomposite.

well-dispersed status of the silica nanoparticles within the polymer matrix, forming a unique nanocomposite.

Rheological Characteristics. Figure S5 (Supporting Information) describes the rheological properties of solution of CMT, CMT-g-PAM, and all nanocomposites in logarithmic scale. It is obvious that all the solutions are pseudoplastic in nature. CMT-g-PAM/SiO_2-3 nanocomposite shows the highest shear viscosity followed by other nanocomposites as well as graft copolymer at both the high and low shear rate regions. It is also mentioned that all the nanocomposites are in a heterophase. So, an increase in solution viscosity clearly implies polymer matrix−nanofiller interaction, generating more restrained graft copolymer segments. The maximum shear viscosity shown by the solution of CMT-g-PAM/SiO_2-3 confirms the presence of a strong graft copolymer−nanosilica interaction at this composition. However, the level of interaction is not so high in CMT-g-PAM/SiO_2-1. This may be because of formation of a separate morphology by the nanosilica. Also, the reason behind the low shear viscosity of CMT-g-PAM/SiO_2-4 solution may be because of the formation of large aggregated silica domains. Another evidence is from the flow behavior index (n, less than 1 indicates pseudoplastic behavior), calculated (Table S1, Supporting Information) using the power law equation:

$$\eta = K\gamma^n \tag{3}$$

where η is the apparent dynamic viscosity at a given temperature, K is consistency coefficient, a value that is proportional to the fluid's viscosity, and γ is the shear rate.

The intercept shows zero shear viscosity which has direct proportionality to the gel microstructure. Slopes of best fitted straight lines indicate a rate of destructuring on shearing. It is assumed that the higher the slope is, the physically weaker is the gel as it loses its structure quite fast. It is found (Table S1, Supporting Information) that the solution of CMT-g-PAM/SiO_2-3 has the lowest "n" values, which elucidates slower polymer matrix−nanosilica disengagements compared to others.

Biodegradation Study. It is observed from Figure S6 (Supporting Information) that CMT, CMT-g-PAM, and CMT-g-PAM/SiO_2-3 are prone to biodegradation as their viscosity decreases gradually. Although the rate of degradation is slightly less for nanocomposite in comparison with CMT and the graft copolymer. This is in agreement with the fact that the developed nanocomposite is biodegradable in nature.

Figure S7 (Supporting Information) shows the fungal growth for various batches of films of CMT-g-PAM/SiO_2-3. It is clearly visible from the figure that apparent fungi growth took place for 0, 7, 14, and 21 days in all the Petri dishes. The growth of fungi in mineral salts agar medium (no carbon content) confirms that the carbon present in the nanocomposite has been utilized by the fungi for its growth. This further confirms the biodegradable nature of the nanocomposite.

Flocculation Characteristics. The flocculation characteristics of CMT, nanosilica, CMT-g-PAM, and all hybrid

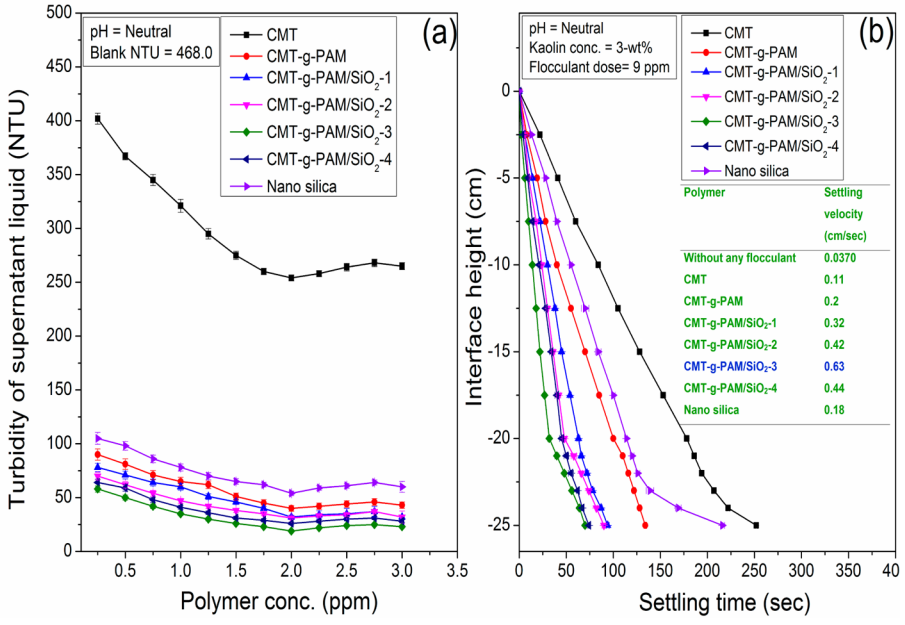

Figure 3. Flocculation characteristics of CMT, CMT-g-PAM, silica particle, and nanocomposites using (a) jar test and (b) settling test (results represented here are ±SD; n = 3).

nanocomposites were investigated using the jar test (Figure 3a) as well as settling test (Figure 3b) in 0.25 wt % and 3 wt % kaolin suspension, respectively. From the figures, it is evident that on addition of polymer- and nanocomposite-based flocculants, the flocculation efficiency increases. The flocculation characteristics of hybrid nanocomposites are better than CMT-g-PAM followed by nanosilica, and CMT. CMT-g-PAM shows better flocculation efficacy due to the presence of flexible polyacrylamide chains onto the rigid polysaccharide backbone. As a result, the approachability of grafted polyacrylamide chains to metallic and nonmetallic contaminants increases significantly.[33] Thus, they are endowed with highly efficient attributes.[34] Further, all nanocomposites show better properties as flocculant in comparison with CMT-g-PAM. This is because of enhancement of hydrodynamic volume (i.e., intrinsic viscosity) as well as hydrodynamic radius on incorporation of nanofiller onto the polymer matrix, which originates from the increased matrix−filler interaction. Now, the higher is the hydrodynamic radius, the higher would be the radius of gyration and hence better will be flocculation efficiency. It has already been established[42] that the higher is the radius of gyration the better would be the flocculation efficiency, as we observed in the case of nanocomposites.

The flocculation performance of a particular polymer is correlated with settling velocity. The higher the settling velocity of the floc containing contaminants, the greater will be its flocculation efficiency. From the settling curves (Figure 3b), it has been observed that the fall of the interface is linear for a considerable height before it becomes nonlinear. This means that the rate of fall of the interface is constant initially, after which it gradually declines. The initial settling rate is calculated from the slope of the linear portion of the settling curves. The settling velocities of kaolin with addition of various flocculants are reported in Figure 3b (inserted onto figure). From the flocculation characteristic studies, it can be concluded that CMT-g-PAM/SiO_2-3 is the best flocculent as it shows the highest settling velocity.

Adsorptions of MB Dye from Aqueous Solution. It is well-known that efficiency of dye adsorption from an aqueous solution of an adsorbent depends on various factors like pH, temperature of the solution, time of adsorption, agitation speed, concentration of dye in the aqueous solution, and amount of adsorbent used.

Effect of pH on Dye Adsorption. The dye adsorption by nanocomposites may be explained by the fact that when a hydrogel is immersed in an aqueous media, it begins to absorb water. This results in considerable change in its network structure. The dye molecules in contact with water may or may not penetrate into hydrogel, depending on the interactions between dye molecules and polymer chains. Generally the adsorption capacity of adsorbent is highly dependent on the pH of the solution. Figure 4 elucidates the effect of pH of the initial dye solution on the adsorption capacity of MB dye onto the CMT-g-PAM/SiO_2-3 nanocomposite for C_0, 50 mg·L^{-1}; adsorbent dose (m), 50 mg/50 mL; temp (T), 40 °C; equilibrium time, 120 min; agitation speed, 100 rpm. It is obvious from Figure 4 that with an increase in pH of the solution from 3.5 to 8.5, the percent adsorption of MB dye increased sharply from 79.34% to 99.76%. It is because of the fact that at pH <6, most of the carboxylate (COO^-) groups of CMT are converted to −COOH groups, which leads to lower MB removal. However, at higher pH, the carboxylic acid groups are ionized and interacted with the dye molecules, which results

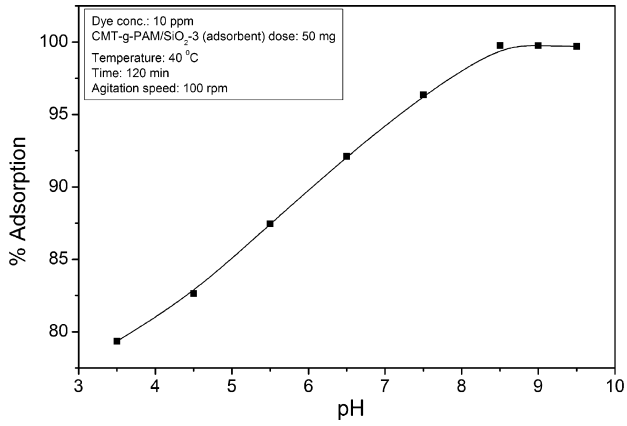

Figure 4. Effect of pH onto percent adsorption of MB dye from an aqueous solution using CMT-g-PAM/SiO_2-3 nanocomposite.

in an increase of the adsorption for MB.[19,43] In addition, at higher pH, the number of ionized groups (COO^-) increased and generated electrostatic repulsive forces among the adjacent ionized groups of the polymer backbone, which results in an expansion of the polymer chains within the nanocomposite structure.[19] This also results in an increase of the adsorption for MB. However, with a further increase in pH beyond 8.5, there is no such increase in percent adsorption, indicating that equilibrium is achieved at pH 8.5. Similar results have been reported for adsorption of MB dye using superadsorbent hydrogel based on modified polysaccharides.[19,43]

Effect of Temperature on Dye Adsorption. The effect of temperature on the adsorption capacity (Figure S8a, Supporting Information) of MB dye by the nanocomposite (CMT-g-PAM/SiO_2-3) has been investigated (for C_0, 50 mg·L^{-1}; adsorbent dose (m), 50 mg/50 mL; pH 8.5; equilibrium time, 120 min; agitation, 100 rpm). The results show that the MB removal capacity increased from 97.45% to 99.76% on increasing temperature from 20 to 40 °C and then decreased up to 98.75% with further rise in temperature till 60 °C. With increase in temperature, the swelling effect within the internal structure of the adsorbent increased, which allow penetration of large dye molecule up to 40 °C.[43,44] However, further increase in temperature increases the mobility of dye molecules, which results lower adsorption efficiency.

Effect of Time on Dye Adsorption. Figure S8b (Supporting Information) illustrates the effect of adsorption time on MB removal efficiency using the CMT-g-PAM/SiO_2-3 nanocomposite. The experimental results indicate that the dye removal rate increases with an increase in adsorption time. The majority of dye removal is achieved in between 90 to 120 min and reaches maximum at 120 min. This phenomenon could be attributed to the instantaneous utilization of the most readily available adsorbing sites on the adsorbent surface. Beyond 120 min, a slower sorption would follow, as the available sorption sites decrease gradually.

Effect of Agitation Speed. It is observed that with an increase in agitation speed from 60 to 100 rpm, % adsorption efficiency increased, beyond which it is decreased (Figure S8c, Supporting Information). This phenomenon could be attributed to the fact that initially on increasing the agitation speed up to 100 rpm, the diffusion rate of MB dye from the bulk liquid to the liquid boundary layer surrounding nanocomposite particles becomes higher because of an enhancement of turbulence. This results in higher adsorption efficiency.

dx.doi.org/10.1021/ie301134a | Ind. Eng. Chem. Res. 2012, 51, 15546−15556

However, beyond the 100 rpm speed, desorption may predominate due to the reverse effect.

Effect of Initial Dye Concentration on MB Adsorption. Figure S8d (Supporting Information) demonstrates the effect of initial concentration of dye on the % adsorption using CMT-g-PAM/SiO_2-3 nanocomposite. It is obvious that with an increase in the initial concentration of MB from 10 to 50 mg/L using a 50 mg adsorbent dose at pH 8.5, the percentage of MB removal decreases from 99.76% to 93.7%. This occurs because at higher MB concentration, the ratio of available adsorbing sites in the adsorbent is fixed and results in a lower percentage of MB removal.

Effect of Adsorbent Content on Dye Adsorption. Figure S8e (Supporting Information) shows the effect of nanocomposite (CMT-g-PAM/SiO_2-3) content on the MB removal efficiency. The content of the nanocomposite significantly affects the removal of dye. The higher dye (99.76%) removal was reached when an intermediate content of the nanocomposite (50 mg) was used. In solution with higher adsorbent content (75−150 mg), lower percent dye removal is observed. This may be because the nanocomposite absorbs preferentially water and later the solute molecule. Accordingly, higher nanocomposite content can absorb a larger amount of water, providing a dye-rich environment.[19]

Consequently optimization of MB dye adsorption from aqueous solution indicates that the maximum dye removal took place from a solution containing 10 ppm dye solution with 50 mg of CMT-g-PAM/SiO_2-3 at 40 °C, 8.5 pH, and at 120 min of contact time with 100 rpm agitation speed.

Adsorption Mechanism. Figure S9 (Supporting Information) elucidates a competitive MB dye adsorption efficiency with time using CMT, graft copolymer, and various nanocomposites (CMT-g-PAM/SiO_2) as adsorbents in the optimized adsorption condition. It is evident that nanocomposites show excellent dye adsorption capacity in comparison to native polysaccharide and graft copolymer. This is because of the higher intrinsic viscosity (i.e., hydrodynamic volume), as well as higher hydrodynamic radius (Table 1) of the nanocomposite. With an increase in hydrodynamic volume and hydrodynamic radius, the availability or accessibility of active sites (carboxylate groups in CMT, carboxylate and amide groups in CMT-g-PAM as well as the nanocomposite) was increased, which improves the adsorption efficiency. Moreover in nanocomposites, the presence of extra −OH groups on silica (silanol group), with respect to CMT and graft copolymer, enhances the adsorption efficiency.

On the basis of above experimental results, we propose a mechanism for high adsorption efficiency of the nanocomposite (Scheme 1). The concentration of silica in the composite matrix also controls the adsorption efficacy. The maximum adsorption was achieved with 1.5 wt % of SiO_2. This is because of uniform distribution of the nanoparticles onto the graft copolymer surface (as evidenced by TEM analysis) and better polymer−SiO_2 nanoparticle interaction (as evidenced by rheological characteristics and ^{13}C NMR analysis).

Adsorption Kinetics. The rate of adsorption is highly dependent on residence time of the dye at the solid−solution interface and diffusion process. To find out the kinetic mechanism of the nanocomposite which controls the adsorption process, the pseudo-first-order,[45] pseudo-second-order,[31,46,47] and second-order models[48] were verified by linear equation analysis: log ($q_e - q_t$) vs t, (t/q_t) vs t, and $1/(q_e - q_t)$ vs t, respectively.

Scheme 1. Schematic Representations of Interaction of MB Dye in Aqueous Solution with (a) CMT, (b) CMT-g-PAM, and (c) CMT-g-PAM/SiO_2-3

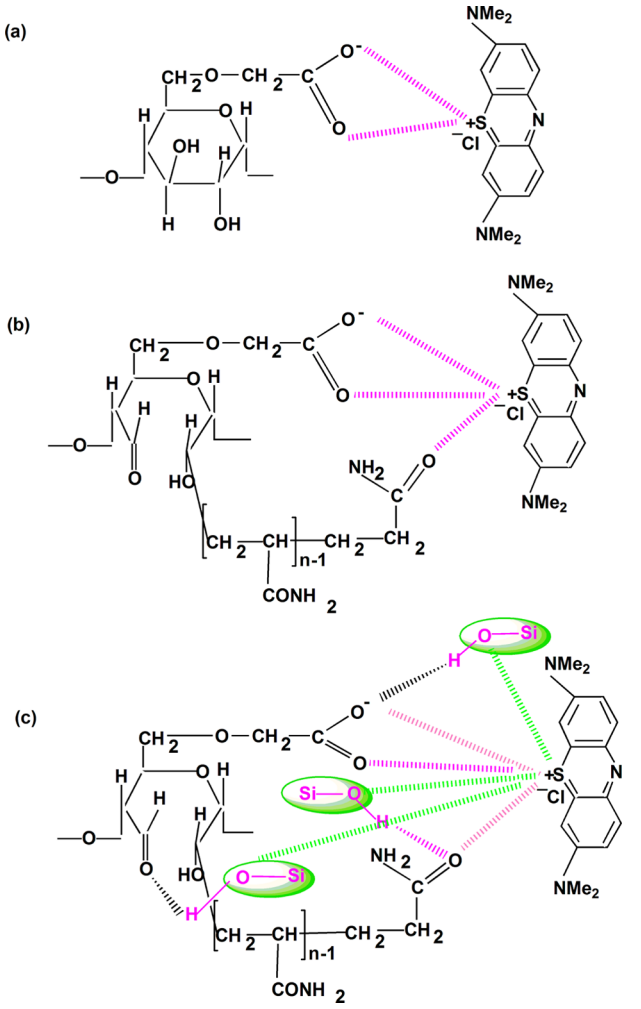

The pseudo-first-order model is one of the most widely used procedures for the adsorption of a solute from aqueous solution.[49] The pseudo-first-order model can be expressed as follows:

$$\log(q_e - q_t) = \log q_e - \frac{k_1}{2.303}t \quad (4)$$

where q_e and q_t (mg/g) refer to the amount of MB adsorbed at equilibrium and time t (min), respectively, k_1 (min^{-1}) is the rate constant. Figure 5a shows the plot for the pseudo-first-order and the parameters k_1, q_e, and the correlation coefficient (R^2) are reported in Table 2.

The pseudo-second-order model is based on the adsorption capacity of solid phase.[50] The model is represented below:

$$\frac{t}{q_t} = \frac{1}{k_2 q_e^{\,2}} + \frac{t}{q_e} \quad (5)$$

where k_2 is the rate constant of pseudo-second-order model (g mg^{-1} min^{-1}). Figure 5b represents the plot for pseudo-second-order and the parameters k_2, q_e, and R^2 values are listed in Table 2.

The second-order rate equation is represented as

dx.doi.org/10.1021/ie301134a | *Ind. Eng. Chem. Res.* 2012, 51, 15546−15556

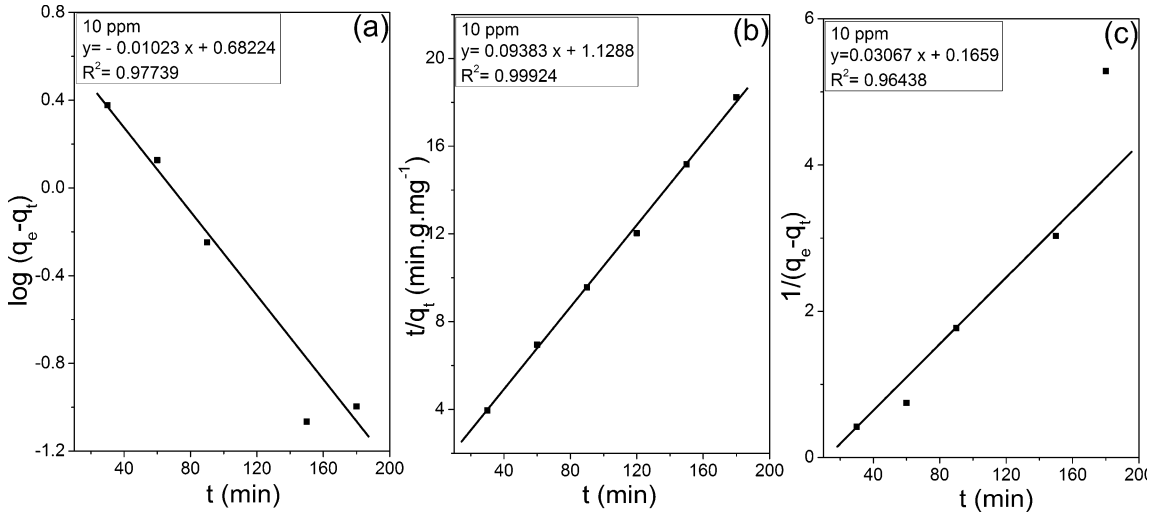

Figure 5. Kinetic modeling of the adsorption of MB dye onto CMT-g-PAM/SiO_2-3 nanocomposite using (a) pseudo-first-order, (b) pseudo-second-order, and (c) second-order models.

Table 2. Kinetic Parameters for the Adsorption of MB Dye from Aqueous Solution Using CMT-g-PAM/SiO_2-3 as Adsorbent

pseudo-first-order model			pseudo-second-order model			second-order model		
K_1 (min^{-1})	q_e ($mg{\cdot}g^{-1}$)	R^2	K_2 ($g{\cdot}mg^{-1}{\cdot}min^{-1}$)	q_e ($mg{\cdot}g^{-1}$)	R^2	K_3 ($g{\cdot}mg^{-1}{\cdot}min^{-1}$)	q_e ($mg{\cdot}g^{-1}$)	R^2
2.356×10^{-2}	4.811	0.97739	7.80×10^{-3}	10.657	0.99924	3.067×10^{-3}	6.027	0.96438

$$\frac{1}{q_e - q_t} = \frac{1}{q_e} + k_3 t \tag{6}$$

where k_3 is the second order rate constant ($g{\cdot}mg^{-1}{\cdot}min^{-1}$). Figure 5c shows the plot for the second order and the parameters k_3, q_e, and R^2 are listed in Table 2.

The R^2 values and the rate constant for all three models suggest that MB dye adsorption using CMT-g-PAM/SiO_2-3 nanocomposite follow pseudo-second-order model; that is, it is dependent on the concentration of dye on the surface of the nanocomposite.

Adsorption Isotherm. The adsorption isotherm shows how the adsorbate molecules are distributed between the liquid phase and solid phase. We have used Langmuir, Freundlich, and Sips isotherm to describe the experimental data. The nonlinear mathematical representation of Langmuir model[51] is

$$q_e = \frac{bQ_0C_e}{1 + bC_e} \tag{7}$$

where C_e is the equilibrium concentration of adsorbate ($mg{\cdot}L^{-1}$), q_e is the amount of dye adsorbed by the composite at equilibrium ($mg{\cdot}g^{-1}$), the Langmuir constant Q_0 ($mg{\cdot}g^{-1}$) represents the monolayer adsorption capacity, and b ($L{\cdot}mg^{-1}$) relates the heat of adsorption. It is well-known that the Langmuir isotherm is valid for monolayer sorption because of the homogeneous surface of a finite number of identical sites. The essential feature of the Langmuir isotherm can be expressed in terms of a dimensionless factor called the separation factor (R_L)[13] which can be explained using the following equation:

$$R_L = \frac{1}{1 + bC_0} \tag{8}$$

where b is the Langmuir constant related to the heat of adsorption and C_0 is the initial dye concentration ($mg{\cdot}L^{-1}$). The value of R_L indicates the shape of isotherm to be either unfavorable ($R_L > 1$), linear ($R_L = 1$), irreversible ($R_L = 0$), or favorable ($0 < R_L < 1$).

A nonlinear form of Freundlich equation[52] is

$$q_e = K_f C_e^{1/n} \tag{9}$$

where K_f ($mg{\cdot}g^{-1}$) and n are Freundlich constants related to the capacity of sorption and favorability of sorption, respectively. The Freundlich isotherm assumes that the dye adsorption occurs on a heterogeneous surface by multilayer sorption.

Meanwhile the nonlinear Sips isotherm model[53] can be considered as a combination of Langmuir and Freundlich equation and represented as below:

$$q_e = \frac{Q_S K_S C_e^{n_S}}{1 + K_S C_e^{n_S}} \tag{10}$$

where Q_S ($mg{\cdot}g^{-1}$) is the specific adsorption capacity at saturation, K_s is the sips isotherm constant related to energy of adsorption and n_S is the heterogeneity factor. If the value of K_S approaches 0, the Sips isotherm will become a Freundlich isotherm. While the value of $n_S = 1$ or closer to 1, the Sips isotherm equation reduces to the Langmuir equation; that is, adsorption takes place on homogeneous surface.[54]

Figure 6 (for temperature 313 K) as well as Table 3 indicate that the Langmuir isotherm model fitted well with the experimental data in comparison to the Freundlich isotherm model, on the basis of the higher correlation coefficient R^2 and lower root-mean-square error (RMSE) values (Figure S10, Supporting Information shows isotherm models at 293 and 303 K). The value of heterogeneity factor ($n_S = 0.992$ at 313 K) of CMT-g-PAM/SiO_2-3 nanocomposite obtained from the Sips model indicates that adsorption took place on the homogeneous surface of a finite number of identical sites. From the Langmuir isotherm (at 293−313 K), Q_0 was found to be 43.859

dx.doi.org/10.1021/ie301134a | Ind. Eng. Chem. Res. 2012, 51, 15546−15556

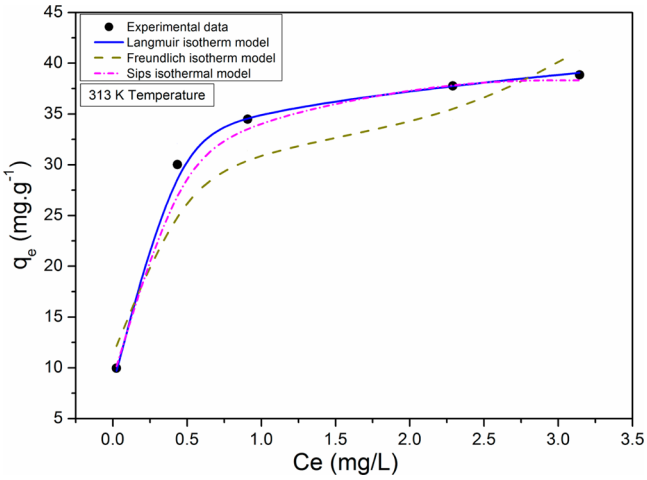

Figure 6. Various isotherm models fit for adsorption of MB dye by CMT-g-PAM/SiO_2-3 nanocomposite at 313 K.

Table 3. Parameters for Langmuir, Freundlich, and Sips Isotherm Model for MB Dye Adsorption Using CMT-g-PAM/SiO_2-3 Nanocomposite As Adsorbent

		temperature		
model	parameter	293 K	303 K	313 K
Langmuir isotherm	Q_{max} (mg·g^{-1})	40.032	40.355	43.859
	b (L·mg^{-1})	1.1614	2.0531	8.4107
	R^2	0.9991	0.9994	0.9997
	RMSE	0.979	0.582	0.395
Freundlich isotherm	K_f (mg·g^{-1})	21.963	24.701	33.412
	n	2.765	3.386	6.066
	R^2	0.9395	0.9625	0.9458
	RMSE	4.208	4.062	4.896
Sips isotherm	Q_s (mg·g^{-1})	38.351	40.750	42.841
	K_s	1.242	1.758	2.122
	n_S	0.974	0.986	0.992
	R^2	0.9745	0.9825	0.9934
	RMSE	1.453	1.281	1.015

mg·g^{-1}. This indicates that the nanocomposite CMT-g-PAM/SiO_2-3 is an efficient adsorbent for removal of a cationic dye (MB dye) from aqueous solution. The values of the Freundlich constant increase with increasing temperature from 20 to 40 °C, suggesting adsorption is endothermic in nature. The Langmuir constant "b" also increases with rising temperature. This explains the stronger affinity between the active sites of the adsorbent and adsorbate as well as between the adjacent molecules of the adsorbed phase at a higher temperature in comparison with a lower temperature. At 10 mg·L^{-1} of MB dye concentration, R_L is calculated and found to be 0.0117 (at 313 K). This confirms that the Langmuir adsorption isotherm is favorable.

Adsorption Thermodynamics. The temperature dependence of adsorption was determined using the Vant Hoff's equation, which is given by

$$\ln b = \frac{\Delta S^0}{R} - \frac{\Delta H^\circ}{RT} \quad (11)$$

$$\Delta G^\circ = \Delta H^\circ - T\Delta S^0 \quad (12)$$

where ΔG° is the change in standard Gibbs free energy (J·mol^{-1}), R is universal gas constant (8.314 J·K^{-1}·mol^{-1}), T is the temperature (K), ΔH° is change in enthalpy (J·mol^{-1}), b is the Langmuir constant at temperature T, and ΔS° is the change in entropy (J·mol^{-1}·K^{-1}). The variation in the extent of adsorption with respect to temperature has been explained based on thermodynamic parameters, namely, change in standard free energy, enthalpy, and entropy. The values of ΔS° and ΔH° were calculated from the intercept and slope of the plot between ln b vs $1/T$ (Figure S11, Supporting Information). The ΔG°, ΔS°, and ΔH° values are listed in Table 4. Negative values of ΔG° indicate the feasibility and spontaneous nature of adsorption process. It may be noted that with an increase in temperature from 293 to 313 K, the ΔG° value decreases (Table 4). This indicates a stronger adsorptive force, which results in a higher degree of spontaneity at higher temperature. The positive value of enthalpy change (ΔH°) confirms the endothermic nature of adsorption process. Positive values of ΔS° suggest good affinity of the dye molecule toward adsorbent.

Table 4. Thermodynamic Parameters for the Adsorption of MB Dye from Aqueous Solution Using CMT-g-PAM/SiO_2-3 Nanocomposite As Adsorbent

temp (K)	ΔG° (KJ·mol^{-1})	ΔH° (KJ·mol^{-1})	ΔS° (KJ·mol^{-1}·K^{-1})
293	−0.18302	53.77	0.18414
303	−2.0244		
313	−3.8658		

Desorption of MB Dye. Desorption studies are extremely useful to find out the suitability of the recycling ability of adsorbent and recovery of the dye. Desorption studies were investigated in various stripping solution with pH = 2.5, pH = 7, and pH = 8.5. Maximum desorption percentage was obtained in an acidic environment (pH = 2.5, 97.80%), and minimum desorption percentage was observed in an alkaline environment (pH = 8.5, 45.50%). Therefore, the exact opposite trend of the adsorption process with pH is followed, as is usually the case. Hence, to determine the reusability of the nanocomposite as adsorbent, four adsorption−desorption cycles were performed with pH = 2.5 as the stripping solution. The desorption study was repeated four times using the same composite and it was found that 91.85% of the MB dye was desorbed after the fourth cycle (Table S2, Supporting Information). The results of the simultaneous four adsorption−desorption cycles are shown in a bar diagram (Figure 7), which indicates the efficient recycling capacity of the synthesized nanocomposite for MB dye separation from water.

CONCLUSION

A novel nanocomposite based on in situ nanofiller (SiO_2) incorporated CMT-g-PAM, with excellent flocculation and dye adsorption efficiency has been successfully synthesized. It is obvious that the concentration of SiO_2 content greatly influences the flocculation as well as adsorption capacity; the best performing nanocomposite being achieved at 1.5 wt % of nanosilica. The high flocculation and adsorption capacity of the nanocomposite is due to its higher hydrodynamic volume, as well as higher hydrodynamic radius, which is generated from the uniform distribution of the nanofiller on the surface of the polymer matrix.

dx.doi.org/10.1021/ie301134a | Ind. Eng. Chem. Res. 2012, 51, 15546−15556

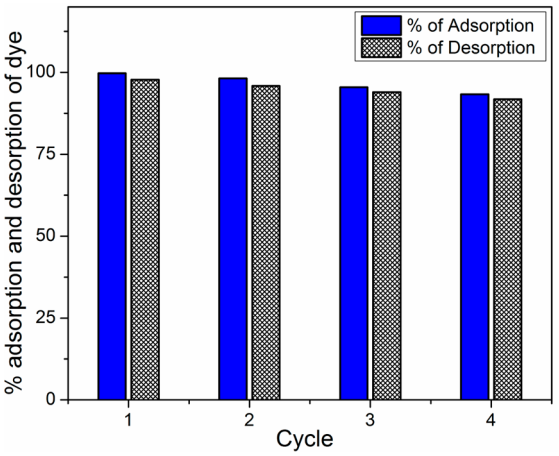

Figure 7. Simultaneous adsorption−desorption cycles using CMT-g-PAM/SiO_2-3 nanocomposite.

■ ASSOCIATED CONTENT

Ⓢ Supporting Information

Detailed procedure for flocculation experiment, adsorption, and desorption study, rheological characteristics, and biodegradation study using a viscometric method as well as a colony growth method; scheme for synthesis of nanocomposite; FTIR analysis; ^{29}Si MAS NMR spectrum of CMT-g-PAM/SiO_2-3; SEM; and EDAX analysis. This material is available free of charge via the Internet at http://pubs.acs.org.

■ AUTHOR INFORMATION

Corresponding Author

*(S.P.) Tel.: 0091-326-2235769. Fax: 0091-326-2296615. E-mail: sagarpal1@hotmail.com. (A.B.P.) Tel: 0091-278-2567760, x704. E-mail: abpanda@csmcri.org.

Notes

The authors declare no competing financial interest.

■ ACKNOWLEDGMENTS

The authors earnestly acknowledge the financial support provided by the Indian School of Mines, Dhanbad, India, in terms of a research grant (Project No. 2010/MRP/AC/05/Acad) to carry out the above investigation. The authors are also thankful to Prof. R. P. Singh, Emeritus Scientist, Indian Institute of Science Education and Research, Pune (IISER, Pune), India, for his kind help.

■ REFERENCES

(1) Pinto, R. J. B.; Marques, P. A. A. P.; Timmons, A. M. B.; Trindade, T.; Neto, C. P. Novel SiO_2/Cellulose Nanocomposites Obtained by in Situ Synthesis and via Polyelectrolytes Assembly. *Compos. Sci. Technol.* **2008**, *68*, 1088.

(2) Marques, P. A. A. P.; Trindade, T.; Neto, C. P. Titanium Dioxide/Cellulose Nanocomposites Prepared by a Controlled Hydrolysis Method. *Compos. Sci. Technol.* **2006**, *66*, 1038.

(3) Li, S. M.; Jia, N.; Ma, M. G.; Zhang, Z.; Liu, Q. H.; Sun, R. C. Cellulose-Silver Nanocomposites: Microwaves-Assisted Synthesis, Characterization, Their Thermal Stability, and Antimicrobial Property. *Carbohydr. Polym.* **2011**, *86*, 441.

(4) Kudaibargenov, S. E.; Tatykhanova, G. S.; Arinov, B. Z.; Kozhakhmetov, S. K.; Aseyev, V. O. Hybrid Inorganic−Organic Nano and Microcomposites Based on Silica Sols and Synthetic Polyelectrolytes. *eXPRESS Polym. Lett.* **2008**, *2*, 101.

(5) Giannelis, E. P. Polymer Layered Silicate Nanocomposites. *Adv. Mater.* **1996**, *8*, 29.

(6) Cheng, Y. J.; Zhou, S.; Gutmann, J. S. Morphology Transition in Ultrathin Titania Films: From Pores to Lamellae. *Macromol. Rapid Commun.* **2007**, *28*, 1392.

(7) Xiao, H.; Cezar, N. Organo-modified Cationic Silica Nanoparticles/Anionic Polymer as Flocculants. *J. Colloid Interface Sci.* **2003**, *267*, 343.

(8) Singh, V.; Kumar, P. Carboxymethyl Tamarind Gum−Silica Nanohybrids for Effective Immobilization of Amylase. *J. Mol. Catal. B* **2011**, *70*, 67.

(9) Singh, V.; Pandey, S.; Singh, S. K.; Sanghi, R. Removal of Cadmium from Aqueous Solutions by Adsorption Using Poly(acrylamide) Modified Guar Gum-Silica Nanocomposites. *Sep. Purif. Technol.* **2009**, *67*, 251.

(10) Nozawa, K.; Gailhanou, H.; Raison, L.; Panizza, P.; Sellier, E.; Ushiki, H.; Delville, J. P.; Delville, M. H. Smart Control of Monodisperse Stober Silica Particles: Effect of Reactant Addition Rate on Growth Process. *Langmuir* **2005**, *21*, 1516.

(11) Lazaridis, N. K.; Kyzas, G. Z.; Vassiliou, A. A.; Bikiaris, D. N. Chitosan Derivatives as Biosorbents for Basic Dyes. *Langmuir* **2007**, *23*, 7634.

(12) Vandevivere, P. C.; Bianchi, R.; Verstraete, W. Review: Treatment and Reuse of Wastewater from the Textile Wet-Processing Industry: Review of Emerging Technologies. *J. Chem. Technol. Biotechnol.* **1998**, *72*, 289.

(13) Ayad, M. M.; El-Nasr, A. A. Adsorption of Cationic Dye (Methylene Blue) from Water Using Polyanilines Nanotubes Base. *J. Phys. Chem. C.* **2010**, *114*, 14377.

(14) Al-Bastaki, N. Removal of Methyl Orange Dye and Na_2SO_4 Salt from Synthetic Wastewater Using Reverse Osmosis. *Chem. Eng. Process: Process Intensif.* **2004**, *43*, 1561.

(15) Namasivayam, C.; Kavitha, D. Removal of Congo Red from Water by Adsorption onto Activated Carbon Prepared from Coir Pith, an Agricultural Solid Waste. *Dyes Pigm.* **2002**, *54*, 47.

(16) Kabra, K.; Chaudhary, R.; Sawhney, R. L. Treatment of Hazardous Organic and Inorganic Compounds through Aqueous-Phase Photocatalysis: A Review. *Ind. Eng. Chem. Res.* **2004**, *43*, 7683.

(17) Mahanta, D.; Madras, G.; Radhakrishnan, S.; Patil, S. Adsorption of Sulfonated Dyes by Polyaniline Emeraldine Salt and Its Kinetics. *J. Phys. Chem. B* **2008**, *112*, 10153.

(18) Annadurai, G.; Chellapandian, M.; Krishnan, M. R. V. Adsorption of Reactive Dye on Chitin. *Environ. Monit. Assess.* **1999**, *59*, 111.

(19) Paulino, A. T.; Guilherme, M. R.; Reis, A. V.; Campese, G. M.; Muniz, E. C.; Nozaki, J. Removal of Methylene Blue Dye from an Aqueous Media Using Superabsorbent Hydrogel Supported on Modified Polysacharide. *J. Colloid Interface Sci.* **2006**, *301*, 55.

(20) Crini, G. Non-conventional Low-Cost Adsorbents for Dye Removal: A Review. *Bioresour. Technol.* **2006**, *97*, 1061.

(21) Gimbert, F.; Crini, N. M.; Renault, F.; Badot, P. M.; Crini, G. Adsorption Isotherm Models for Dye Removal by Cationized Starch-Based Material in a Single Component System: Error Analysis. *J. Hazard. Mater.* **2008**, *157*, 34.

(22) Crini, G.; Badot, P. M. Application of Chitosan, a Natural Amino Polysaccharide, for Dye Removal from Aqueous Solutions by Adsorption Processes Using Batch Studies: A Review of Recent Literature. *Prog. Polym. Sci.* **2008**, *33*, 399.

(23) Renault, F.; Crini, N. M.; Gimbert, F.; Badot, P. M.; Crini, G. Cationized Starch-Based Material as a New Ion-Exchanger Adsorbent for the Removal of C.I. Acid Blue 25 from Aqueous Solutions. *Bioresour. Technol.* **2008**, *99*, 7573.

(24) Yi, J. Z.; Zhang, L. M. Removal of Methylene Blue Dye from Aqueous Solution by Adsorption onto Sodium Humate/Polyacrylamide/Clay Hybrid Hydrogels. *Bioresour. Technol.* **2008**, *99*, 2182.

(25) Crini, G. Recent Developments in Polysaccharide-Based Materials used as Adsorbents in Wastewater Treatment. *Prog. Polym. Sci.* **2005**, *30*, 38.

(26) Parasuraman, D.; Serpe, M. J. Poly(*N*-isopropylacrylamide) Microgel-Based Assemblies for Organic Dye Removal from Water. *ACS Appl. Mater. Interface* **2011**, *3*, 4714.

(27) Konaganti, V. K.; Kota, R.; Patil, S.; Madras, G. Adsorption of Anionic Dyes on Chitosan Grafted Poly(alkylmethacrylate)s. *Chem. Eng. J.* **2010**, *158*, 393.
(28) Singh, V.; Sharma, A. K.; Tripathi, D. N.; Sanghi, R. Poly(methylmethacrylate) Grafted Chitosan: An Efficient Adsorbent for Anionic Azo Dyes. *J. Hazard. Mater.* **2009**, *161*, 955.
(29) Singh, V.; Sharma, A. K.; Sanghi, R. Poly(acrylamide) Functionalized Chitosan: An Efficient Adsorbent for Azo Dyes from Aqueous Solutions. *J. Hazard. Mater.* **2009**, *166*, 327.
(30) Sanghi, R.; Bhattacharya, B.; Singh, V. Seed Gum Polysaccharides and their Grafted Co-polymers for the Effective Coagulation of Textile Dye Solutions. *React. Funct. Polym.* **2007**, *67*, 495.
(31) Ho, Y. S.; Chiang, T. H.; Hsueh, Y. M. Removal of Basic Dye from Aqueous Solution Using Tree Fern as a Biosorbent. *Process Biochem.* **2005**, *40*, 119.
(32) Pal, S.; Ghorai, S.; Dash, M.; Ghosh, S.; Udayabhanu, G. Flocculation Properties of Polyacrylamide Grafted Carboxymethyl Guar Gum (CMG-g-PAM) Synthesized by Conventional and Microwave Assisted Method. *J. Hazard. Mater.* **2011**, *192*, 1580.
(33) Singh, R. P.; Karmakar, G. P.; Rath, S. K.; Karmakar, N. C.; Pandey, S. R.; Tripathy, T.; Panda, J.; Kannan, K.; Jain, S. K.; Lan, N. T. Biodegradable Drag Reducing Agents and Flocculants Based on Polysaccharides: Materials and Applications. *Polym. Eng. Sci.* **2000**, *40*, 46.
(34) Singh, R. P.; Pal, S.; Krishnamoorthy, S.; Adhikary, P.; Ali, S. K. High Technology Materials Based on Modified Polysaccharides. *Pure Appl. Chem.* **2009**, *81*, 525.
(35) Pal, S.; Pal, A. Synthesis and Characterizing a Novel Polymeric Flocculant Based on Amylopectin-Graft-Polyacrylamide-Graft-Polyacrylic Acid [(AP-g-PAM)-g-PAA]. *Polym. Bull.* **2012**, *69*, 545.
(36) Brostow, W.; Lobland, H. E. L.; Reddy, T.; Singh, R. P. Lowering Mechanical Degradation of Drag Reducers in Turbulent Flow. *J. Mater. Res.* **2007**, *22*, 56.
(37) Sumathi, S.; Ray, A. R. Release Behavior of Drugs from Tamarind Seed Polysaccharide Tablets. *J. Pharm. Sci.* **2002**, *5*, 12.
(38) Marathe, R. M.; Annapure, U. S.; Singhal, R. S.; Kulkarni, P. R. Gelling Behaviour of Polyose from Tamarind Kernel Polysaccharide. *Food Hydrocolloids* **2002**, *16*, 423.
(39) Pal, S.; Sen, G.; Mishra, S.; Dey, R. K.; Jha, U. Carboxymethyl Tamarind: Synthesis, Characterization and its Application as Novel Drug-Delivery Agent. *J. Appl. Polym. Sci.* **2008**, *110*, 392.
(40) Sen, G.; Pal, S. Polyacrylamide Grafted Carboxymethyl Tamarind (CMT-g-PAM): Development and Application of a Novel Polymeric Flocculant. *Macromol. Symp.* **2009**, *277*, 100.
(41) Sen, G.; Ghosh, S.; Jha, U.; Pal, S. Hydrolyzed Polyacrylamide Grafted Carboxymethylstarch (Hyd. CMS-g-PAM): An Efficient Flocculant for Treatment of Textile Industry Wastewater. *Chem. Eng. J.* **2011**, *171*, 495.
(42) Brostow, W.; Pal, S.; Singh, R. P. A Model of Flocculation. *Mater. Lett.* **2007**, *61*, 4381.
(43) Wang, L.; Zhang, J.; Wang, A. Removal of Methylene Blue from Aqueous Solution Using Chitosan-g-poly(acrylic acid)/Montmorillonite Superadsorbent Nanocomposite. *Colloids Surf. A* **2008**, *322*, 47.
(44) Bhattacharya, K. G.; Sharma, A. Adsorption Characteristics of the Dye, Brilliant Green, on Neem Leaf Powder. *Dyes Pigm.* **2003**, *57*, 211.
(45) Chiou, M. S.; Li, H. Y. Equilibrium and Kinetic Modeling of Adsorption of Reactive Dye on Cross-Linked Chitosan Beads. *J. Hazard. Mater.* **2002**, *93*, 233.
(46) Ho, Y. S.; Wase, D. A. J.; Forster, C. F. Batch Nickel Removal from Aqueous Solution by Sphagnum Moss Peat. *Water Res.* **1995**, *29*, 1327.
(47) Ho, Y. S.; McKay, G. The Kinetics of Sorption of Divalent Metal Ions onto Sphagnum Moss Peat. *Water Res.* **2000**, *34*, 735.
(48) Ho, Y. S. Second-Order Kinetic Model for the Sorption of Cadmium onto Tree Fern: A Comparison of Linear and Non-linear Methods. *Water Res.* **2006**, *40*, 119.
(49) Ho, Y. S.; McKay, G. A Comparison of Chemisorptions Kinetic Models Applied to Pollutant Removal on Various Sorbents. *Trans. IChemE.* **1998**, *76B*, 332.
(50) Ho, Y. S.; Wase, D. A. J.; Forster, C. F. Kinetic Studies of Competitive Heavy Metal Adsorption by Sphagnum Moss Peat. *Environ. Technol.* **1996**, *17*, 71.
(51) Langmuir, I. The Constitution and Fundamental Properties of Solids and Liquids. *J. Am. Chem. Soc.* **1916**, *38*, 2221.
(52) Freundlich, H. M. F. Über Die Adsorption in Lösungen. *Z. Phys. Chem.* **1906**, *57*, 385.
(53) Sips, R. On the Structure of a Catalyst Surface. *J. Chem. Phys.* **1948**, *16*, 490.
(54) Chatterjee, S.; Lee, M. W.; Woo, S. H. Adsorption of Congo Red by Chitosan Hydrogel Beads Impregnated with Carbon Nanotubes. *Bioresour. Technol.* **2010**, *101*, 1800.